NPL REPORT
DQL-AC 012

Towards a calibrated reference source for in-situ calibration of acoustic emission measurement systems

Pete Theobald and Alex Thompson

NOT RESTRICTED

FEBRUARY 2005

Towards a calibrated reference source for in-situ calibration of acoustic emission measurement systems

Pete Theobald and Alex Thompson
Quality of Life Division

ABSTRACT
Despite the long-standing application of acoustic emission (AE) testing, agreed measurement standards and a traceable measurement infrastructure have yet to be established. This has undoubtedly limited the applicability of AE measurements on safety critical structures. The accepted method of characterising the measurement system, often termed system calibration, is the Hsu-Neilsen pencil lead break. NPL is undertaking work to develop a reference source that will provide a traceable alternative to the pencil lead break and add an element of traceability to this system calibration. This will contribute to greater acceptance of AE techniques in general, by meeting quality system and other traceability requirements.

This report proposes a methodology for the calibration of a conical piezoelectric transmitter against a laser interferometer for use as a reference source. A typical calibration of this reference source has been demonstrated which provides a known output displacement for a given drive voltage. This type of traceable reference source could be used for system calibration in place of a Hsu-Neilsen pencil lead break.

This report is the deliverable for milestone 2.4.01.8 of the National Measurement System NMS 2001-2004 Acoustical Metrology Programme entitled 'Development of a calibrated reference source for in-situ calibration of acoustic emission measurement'.

ISSN 1744-0599

National Physical Laboratory
Hampton Road, Teddington, Middlesex, TW11 0LW

Approved on behalf of the Managing Director, NPL
by Dr B Zeqiri, authorised by Director for Quality of Life Division

CONTENTS

1 INTRODUCTION

1.1 Acoustic emission background

Acoustic emission (AE) refers to sounds, in the form of acoustic and ultrasonic energy, emitted from either a material or a structure which can provide diagnostic information about the state of that material or structure. AE differs from other non-destructive testing (NDT) techniques in two main respects: firstly, the energy is released from within the test object itself; and secondly, AE is capable of detecting dynamic processes associated with the degradation of structures, such as crack growth or plastic deformation. AE makes use of the fact that localised discontinuities will appear long before a structure fails. Monitoring of items such as crack growth gives the maintenance engineer a very useful tool. It prevents the need for unnecessary and expensive early shut-down of plant, as well as providing the means to minimize expensive, and often dangerous, failures. Recently, interest has increased in the use of AE as an in-service condition monitor and as an on-line process monitoring technique. Examples cover a wide spectrum of applications, from monitoring of large pressure vessels, storage tanks, and large structures such as bridges and aircraft structures, to studying tool wear and compositions of liquids.

Although AE has been used for many years, the last ten years has seen increased computing power enable advances in signal processing such that the reliability of the AE technology is now recognised by a wider range of industries. Furthermore, the need for quality control at the manufacturing stage and during in-service testing has encouraged the issue of traceable measurements to be addressed.

1.2 Project details

This milestone aims to establish a measurement facility, investigate the use of a suitable reference source for acoustic emission measurement system calibration and investigate a methodology for the calibration of the reference source. The milestone entitled ‘Development of a calibrated reference source for in-situ calibration of acoustic emission measurement systems’ is Milestone 2.4.01.8 of the National Measurement System (NMS) 2001-2004 Acoustical Metrology Programme of the UK Department of Trade and Industry.

1.3 System calibration background

System calibration or the testing of an acoustic emission measurement system is required due to the wide range of the structures on which acoustic emission measurement techniques are used. The sensors used for acoustic emission detection are generally calibrated on a suitable reference block, with a particular coupling material for their response to a given wave mode. When used on the measurement structure, the sensors are coupled to different materials, with different acoustic load impedances, using different coupling materials on surfaces that can often lead to very inconsistent coupling qualities. Furthermore, the generated surface displacement to which the sensor responds is never completely understood, being made up of vector components which depend on the type of wave mode and the incidence at which it arrives at the surface. One can therefore never be sure how the measurement system is performing for a given test, particularly if the sensors have been removed and re-coupled as would be the case for a periodic test.

For many years the internationally accepted method for testing an AE measurement system has been the Hsu-Neilsen pencil lead break [1]. Its use was initially proposed to provide a step-force point source input function for the calibration of sensors. However, it has also been used for the in-situ verification of sensor operation, coupling and response of measurement systems, which is often inaccurately referred to as 'system calibration'. The standard procedure for this 'calibration' is to position the Hsu-Neilson source a set distance from the acoustic centre of each sensor and measure the output level for each, ensuring that it is above a pre-defined threshold. Its ease of use in practice has led to widespread acceptance of the source for the in-situ 'calibration' of AE measurement systems.

Although this method is still very useful for characterising an AE measurement system to a step-force function input, it does not offer traceability to fundamental standards and therefore cannot meet all the demands of modern AE applications which require such traceability. Ideally, a system calibration would enable a comparison of the state of a measurement system with another; these might be identical measurement systems at discrete locations or the same measurement system performing measurements on a periodic basis. A typical example of this might be the periodic testing of an engineering structure where the sensors are removed between tests. To allow comparison between the results from successive tests, the person performing the measurement needs to be confident that the measurement system is setup and performing the same as it was in previous tests. The absence of traceability when using the pencil lead break for the in-situ 'calibration' of the measurement system means that this confidence cannot be realised.

There have been a number of research activities presented in the literature which have proposed methods for system calibration. Many of these are based on energy calibration methods, employing a quantitative source and using the linear relationship between the stress wave energy generated and the electrical energy generated at the sensor [2]. Both the elastic ball impact and the thermoelastic laser pulse have been used as a quantitative source [3,4,5]. The stress wave energy generated in the samples by the ball impact was calculated from the loss in potential energy on impact, thus assuming a perfectly elastic impact. Similarly, the pulsed laser was assumed to be a perfectly thermoelastic interaction with all the laser energy being absorbed within the skin depth of the material such that the surface heat increase was fully converted into a volume increase at the surface of the material [6]. The ball impact and the high power pulsed laser are problematic due to difficulties in transferring the calibration to a real AE measurement environment, and limited due to the assumptions made in calculating the energy injected into the structure. More recent work has been undertaken on the use of a conical transducer as a transfer source with its output compared to that of a ball impact to provide a known energy input to the sample [7]. The limitations with such a calibration method are assumptions already mentioned regarding the elastic ball impact and the difficulty in comparing the two sources given their differing interaction mechanisms.

1.4 Rationale for NPL calibrated reference source

The strategy adopted within this milestone is to use a conical type transducer as described in Section 2.1 and to calibrate it using optical interferometry such that it produces a known acoustic displacement for a given input voltage [8].

Such methodology provides a reference source traceable to standard units that can be used to test or calibrate acoustic emission measurement systems. This approach offers a more metrologically sound 'calibration' than the Hsu-Neilson pencil lead break and should allow the performance of a measurement system to be established with a stated random uncertainty, allow greater comparison between periodic testing of a structure. Ultimately, such a reference source would be used on systems with calibrated sensors traceable to international standards, enabling traceable linkages at each stage of the measurement chain and thus providing greater measurement confidence.

2 PROPOSED REFERENCE SOURCE

2.1 Conical transducer design

The transmitter characterised in this report is the conical piezoelectric transducer, which was originally proposed by NIST as a broadband point contact reference sensor [10,11] and was further improved in subsequent work by NIST [12,13]. The NIST reference sensor consisted of a 2.5 mm thick lead-zirconate-titanate (PZT) conical element with a truncated contact point, 1.5 mm in diameter. A large brass cylinder measuring 37 mm in diameter and 25 mm in length was used as the mass backing with rounded edges on the face contacting the PZT element. The size of the backing served to reduce the extent of the axial and thickness modes in the piezoelectric element by delaying the internal reflections that impinge on the back of the element enough to remove them from the time frame of the signal of interest [10]. The NIST design achieved a broad measurement bandwidth within ± 3 dB between 50 kHz and 1 MHz with very little compromise in sensitivity compared with a standard AE type sensor at the time. Other designs of point contact transducers have lead to improvements over the NIST design. AEA Harwell designed a small conical transducer with a tear drop shaped brass backing that showed significant sensitivity up to 2 MHz and a limited response up to 10 MHz [14], whilst maintaining a sensitivity comparable to that of the NIST reference sensor when calibrated using a pulsed laser source and a capacitance transducer. Other variations of the conical design have also been explored in the literature [15] and laser-machining techniques have been used to produce broad bandwidth miniature conical transducers [16,17].

The actual transducer used for the work presented in this report was a modified design manufactured by Imperial College, UK, employing a 3 mm thick conical piezoelectric element with a top diameter of 10 mm and a surface contact diameter of 1 mm [18,19]. The piezoelectric element was mass loaded with a 14 mm layer of tungsten-loaded epoxy and a 14 mm layer of pure epoxy backing layer with a 20 mm diameter as shown in Figure 1.

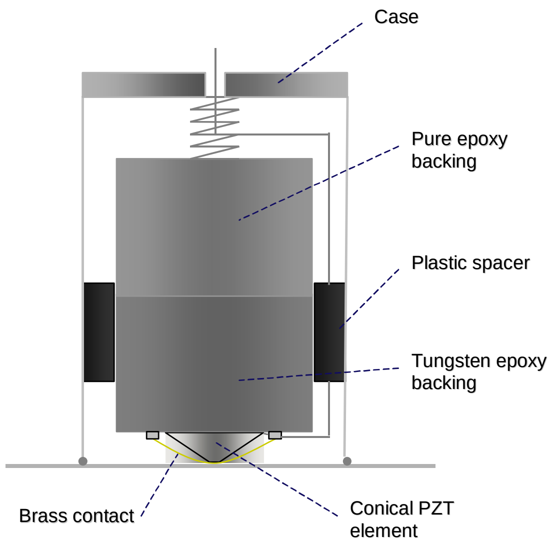

Figure 1. Construction of tungsten loaded epoxy backed conical transducer.

The tungsten loaded epoxy and pure epoxy backing was used to provide maximum suppression of internal reflections and provide a good acoustic impedance match with the piezoelectric element [18]. The wave speeds in tungsten epoxy are much less than those of brass so the backing provided an increased delay of internal reflections when compared with a similar brass backed transducer. A measurement bandwidth in excess of 1 MHz was demonstrated with a very smooth, damped response [18]. The transducer was designed to contact the surface via a 50 µm brass shim which provides both the electrical earth and a protective wear layer for the piezoelectric element. The transducer design also incorporates a spring to maintain the contact force of the active element when the transducer case is secured to the surface.

The small contact area of such a transducer design reduces aperture effects and coupling variability [18], and although a conical element has more mechanical resonances than a disc-shaped element, these resonances are less dominant, giving such transducers an improved broadband frequency response. The tungsten loaded epoxy and pure epoxy backing further dampen the response of the conical piezoelectric element by reducing internal reflections.

2.2 Transducer testing

To test its performance as a transmitter, both a conical transmitter (Tx2) and a nominally identical conical receiver (Rx1) were coupled to the flat surface of the NPL aluminium test cylinder which has a diameter of 254 mm and a length 279 mm as shown in Figure 2. The dimensions of the cylinder allow windowing of the direct surface wave before reflections from the side or the bottom of the block arrive.

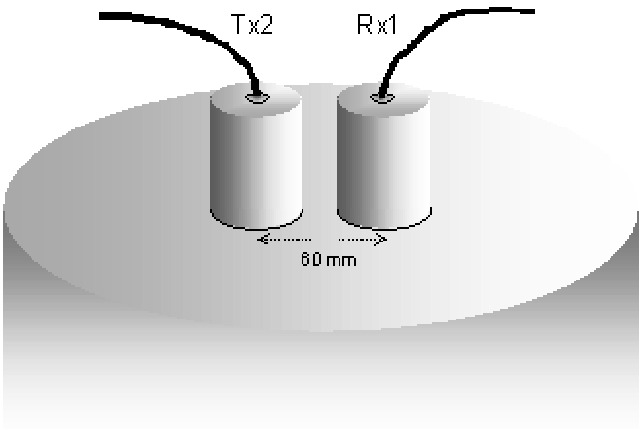

Figure 2. Conical transmitter and receiver arrangement on aluminium cylinder.

The output of the conical receiver Rx1 was connected to a Physical Acoustics AECL 2100/PA pre-amplifier unit with a 60 dB gain and 20 kHz to 1.2 MHz bandpass filter and sampled using a Hewlett Packard HP89410A vector signal analyser with a sample rate of 25.6 MS/s. To drive the transmitter, an arbitrary pulse generator was used with an integrated 40 dB power amplification unit to drive the transmitter up to 100 $V_{p\text{-}p}$. The input signal supplied to the transmitter Tx2 was also captured using the HP89410A via the pre-amplification monitor. To test the conical transducer, a 5 cycle Hanning windowed tone-burst was used with centre frequencies of 150 kHz, 300 kHz, 500 kHz and 1000 kHz which are shown in Figures 3a to 6a respectively along with the respective receiver outputs of the surface wave in Figures 3b to 6b. A single sine wave pulse was also used centred at 500 kHz as shown in Figure 7a with the respective receiver output in Figure 7b. Figure 8a shows an approximation of a delta function input with a pulse width of 1 µs with the receiver output shown in Figure 8b. The FFT’s for both the input and output time waveforms shown in Figures 3 to 8 are shown in Figure 3c to 8c respectively. The dashed line shows the FFT of the input signal produced by the function generator and the solid line shows the FFT of the conical transmitter output.

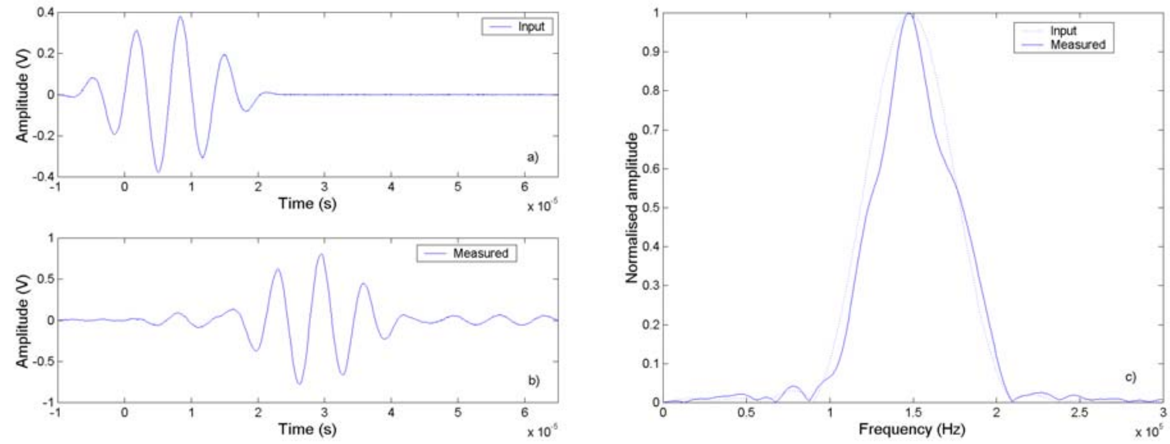

Figure 3. a) 150 kHz input toneburst to transducer. b) Conical receiver output signal. c) FFT of input and received signals.

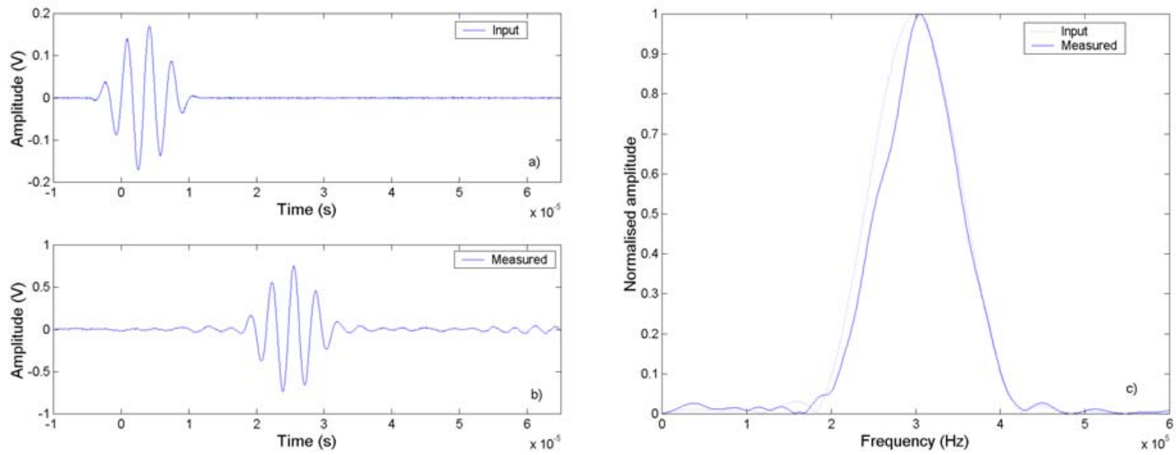

Figure 4. a) 300 input toneburst to transducer. b) Conical receiver output signal. c) FFT of input and received signals.

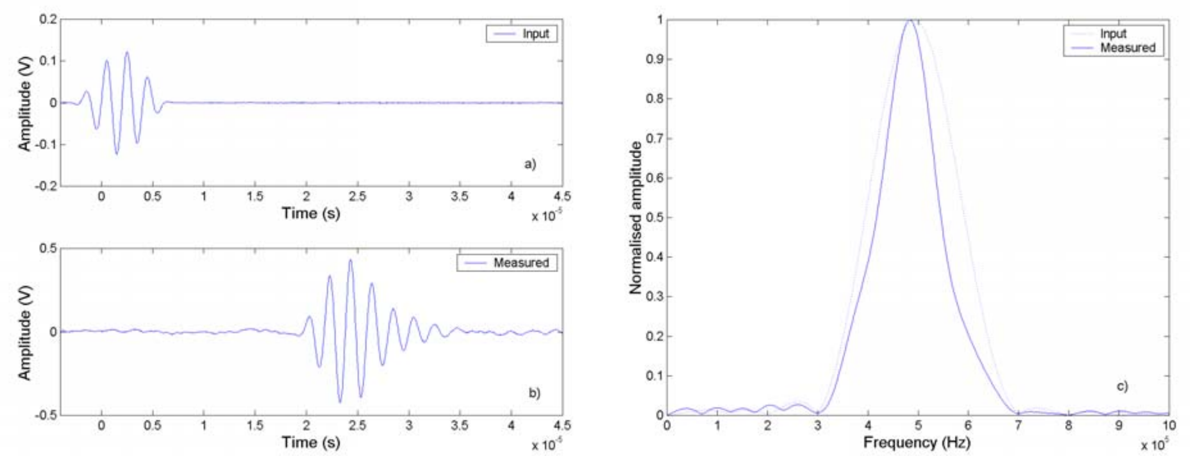

Figure 5. a) 500 kHz input toneburst to transducer. b) Conical receiver output signal. c) FFT of input and received signals.

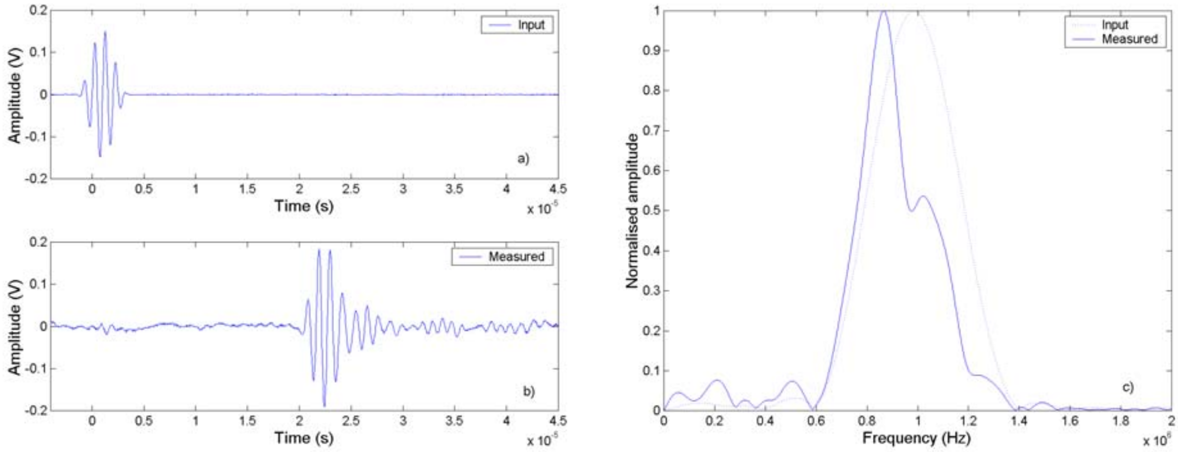

Figure 6. a) 1 MHz input toneburst to transducer. b) Conical receiver output signal. c) FFT of input and received signals.

The reproduction of the drive wave form is excellent at 150 kHz and 300 kHz, showing only a small amount of ringing at 500 kHz. The frequency response matches very closely the frequency spectrum of the input waveform which is excellent considering it is a result of the transfer function of both the transmitter, the receiver, the pre-amp/filter unit and propagation in the material. This shows that the transducer performs well as a transmitter (and a receiver) and is capable of accurately reproducing waveforms with in its operational frequency range. The limitations above 1 MHz can be seen from Figure 6, although it should be noted that this limitation could be imposed by the pre-amp/filter unit.

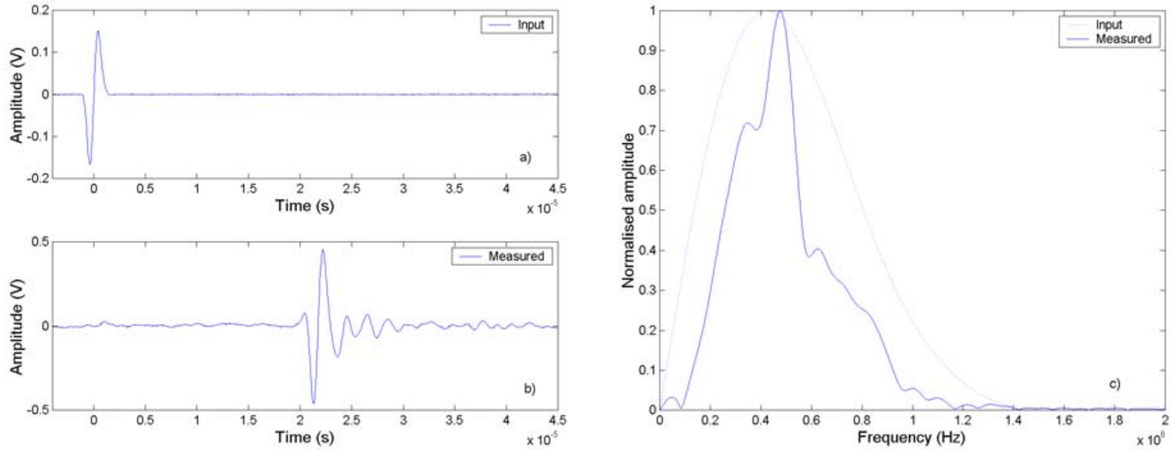

Figure 7. a) 0.5 MHz single cycle input to transducer. b) Conical receiver output signal. c) FFT of input and received signals.

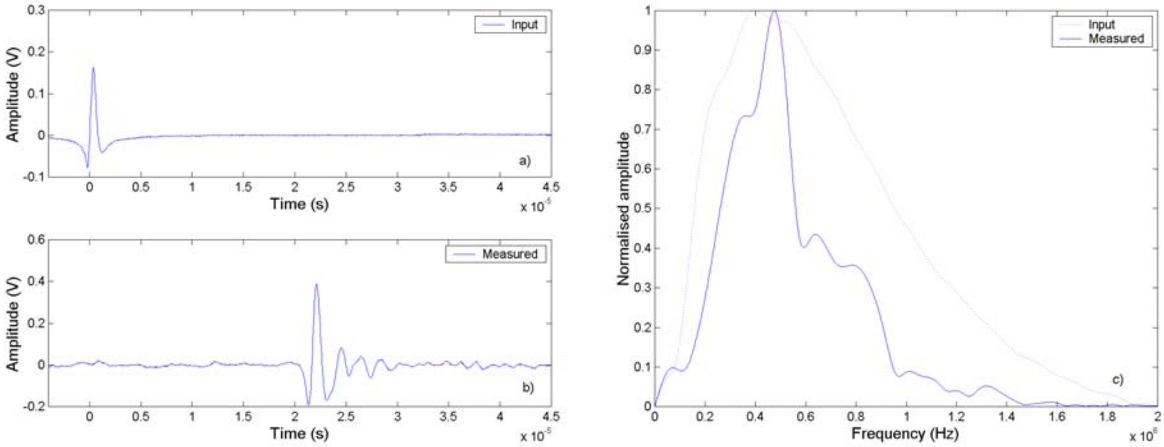

Figure 8. a) 1 μs pulse input to transducer. b) Conical receiver output signal. c) FFT of input and received signals.

The single cycle and the square pulse input to the transducer show a small amount of ringing at the receiver output, see Figure 7b and 8b. The spectra shown in Figure 7c and 8c are a result of both the transmitter transfer function, the receiver transfer function and the pre-amp/filter unit transfer function. To represent the response of the transmitter the square-root of the FFT of the received signal is shown in Figure 9. This makes the assumption that the transducer is completely reciprocal and effectively treats the receiver and pre-amp/filter unit as a single combined transfer function. It does however show that the transmitter is capable of reproducing the square pulse input signal with significant acoustic output above 1 MHz.

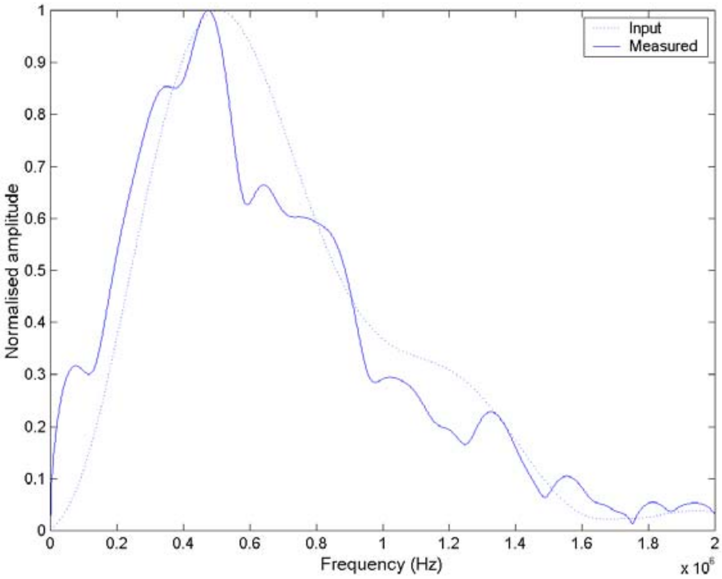

Figure 9. Square-root of measured response compared with response of square input pulse.

The broadband response of the conical transducer, the controllability of input pulse characteristics, the control over the input magnitude and its point contact, make it an ideal reference source for system testing and calibration.

3 CALIBRATION EQUIPMENT AND METHODOLOGY

3.1 Interferometer design and development

The basic interferometer specification was initially generated as part of a collaborative project with Lloyd's Register of Shipping and Airbus UK in the 1998-2001 DTI NMS Acoustical Metrology Programme. One requirement was for a bandwidth of 20 kHz to 3 MHz. Furthermore, it was stated the noise equivalent displacement should be a maximum of 10 pm RMS with a target maximum of 5 pm RMS in the absence of intermode beats, measured on a high quality target mirror with reflectance greater than 90%.

The interferometer uses a 633 nm wavelength helium neon laser as a coherent light source. The operation of the interferometer is straightforward. Light reflected from a vibrating object is mixed with a reference beam on a photodetector. The path length difference between the target and reference beam is held constant by a servo-driven path length compensator, giving phase quadrature between the beams. The system acts as a phase or path length discriminator for frequencies higher than the response speed of the compensator, with the photodetector current being proportional to the displacement of the target, provided that the displacements are small and there is a constant returned light level.

As the returned light level can vary, an automatic calibration technique is used to maintain constant output sensitivity. This is done by injecting a phase modulation equivalent to a target displacement of 40 nm at 14.74 MHz. An automatic gain controlled amplifier maintains a constant level of the 14.74 MHz signal at the output. A low pass filter is then used to eliminate this calibrator signal from the output. The second harmonic of the calibrator signal, 29.48 MHz, is phase detected against a 29.48 MHz reference to provide a control signal for the path length compensator system.

Two test functions are provided allowing the system calibration to be checked. The first involves the injection of a cyclic displacement of the compensator to display quarter-wave output signals representing a 158 nm peak-to-peak displacement. The second applies a test signal of 25 kHz to the modulator crystal, giving a signal equivalent to 2.5 nm peak-to-peak of target displacement. Figure 10 shows a schematic diagram of the interferometer's basic components.

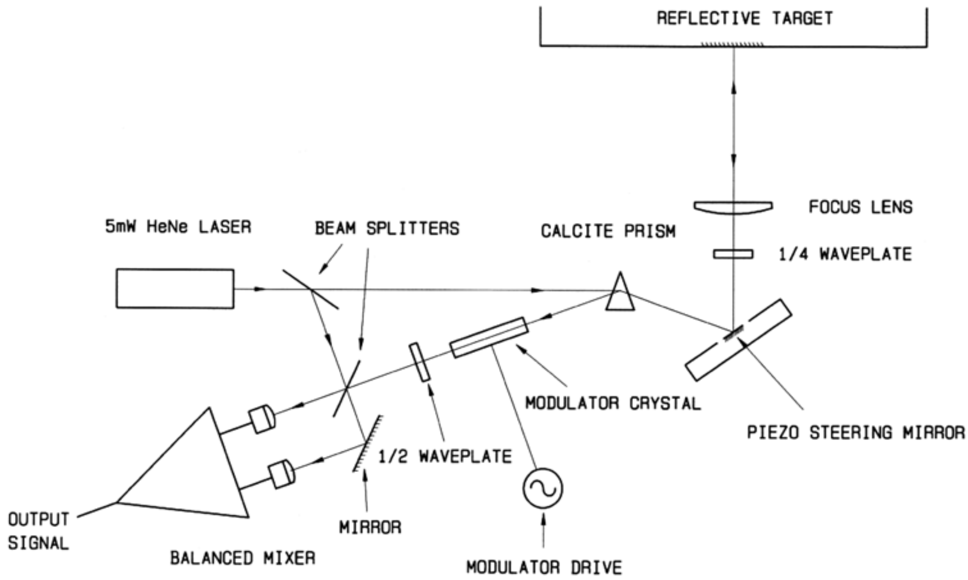

Figure 10. Basic components of interferometer system.

The Photometric Consultants Limited (PCL) interferometer was originally provided with a standard Lasos LGR 7628-1 He-Ne laser tube. The presence of multiple length modes in the laser cavity produced low frequency beat frequencies between the basic frequency modes of the laser. This effect was undesirable as the interferometer would only be useable in a non-moding state, which would normally be around 50% of the operational time. The time period of the moding and non-moding states also increased as the rate of temperature-increase of the laser tube decreased, leading to unusable periods of up to 45 minutes. To remove this effect, modifications were made to the laser tube to stabilise the cavity length and thus the basic frequency mode of the laser. This modification was performed by PCL in two steps. The first step was to control the temperature of the laser tube and thus stabilise the cavity length. This was achieved by fitting a feedback controlled heating coil around the laser tube. The second step was to provide absolute laser cavity length stabilisation; achieved by fitting a piezoelectric actuator at one end of the cavity to hold the cavity length stable in a non-moding state. The specification for the modification stated that a minimum 2-hour useable period of operation was required after a 20 minute warm up period with a possible short un-useable period at the end of the 2-hour period for resetting of the feedback and locking circuit. This specification was met and provided extended measurement times of greater than 2 hours.

Following acceptance, the noise floor of the interferometer was extensively evaluated and the displacement equivalent noise floor was found to be typically better than the specified 5 pm RMS, giving results as low as 3.5 pm RMS from a reference mirror. An assessment of the interferometer's spectral noise content was performed to establish any sources of noise through consultation with PCL, exploring possibilities of filtering to improve the noise floor and to identify consistent components that could not be removed by averaging. Since many of the measurements performed using the interferometer are in the picometer range, they are often heavily reliant on averaging to extract the signal from the noise floor. Many of the initial spectral analysis measurements indicated a number of interference components at 1.34 MHz, 3.75 MHz, 4.77 MHz, 12.12 MHz and 14.74 MHz. The specified measurement bandwidth of the interferometer was 20 kHz to 3 MHz, so low pass filters could be applied above 3 MHz to remove any unwanted components. Noise was also present at lower frequencies, generally around 3 kHz whose source could not be identified. It is probable this was external noise. The most dominant component measured was around 1.34 MHz and often varied in amplitude depending on how long the laser had been running, see Figure 11.

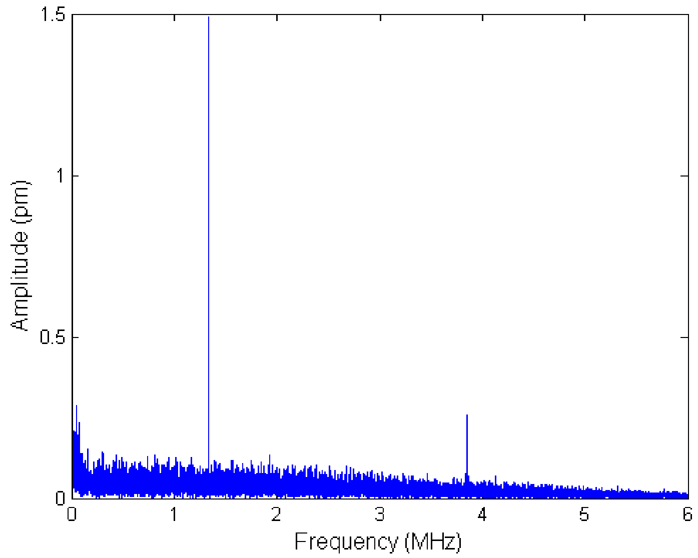

Figure 11. Single shot noise spectra of interferometer noise before modification.

Although the presence of the 1.34 MHz noise component did not compromise the specified noise floor, it was a limiting factor when using averaging to measure displacement components buried in the noise floor. The source of the noise was investigated by PCL and identified as being caused by a gas resonance within the laser. Modifications were carried out by PCL to reduce the noise component. This was achieved by reducing the laser drive current from 6.5 mA to 6 mA. The noise spectra following the modification is shown in Figure 12.

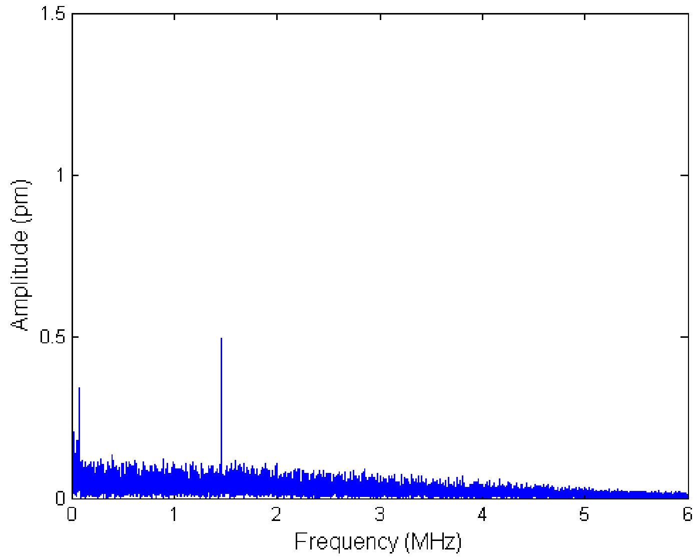

Figure 12. Single shot noise spectra of interferometer noise following modification.

3.2 Test block

Although it might seem preferable to employ metals as test block materials for acoustic emission, it was decided that glass would be used as the test block material. The main reason for this being its optically transparent properties which allows the laser interferometer beam to be directed through the block to measure displacement at any surface of interest. Glass is easy to polish and coat to provide a suitable surface for the optimum reflection of the laser signal.

The test block used was produced using Schott NBK7 standard optical quality borosilicate glass with approximate dimensions 240 mm by 250 mm by 160 mm and is shown in Figure 13. The preparation of this glass test block has been described in a previous report [19] where the block's homogenous properties were characterised to provide an estimated longitudinal wave speed of $6014 \pm 17\ ms^{-1}$.

The initial coating was of aluminium to provide maximum reflection and thus sensitivity of the interferometer. However, the aluminium proved to be too soft, with coupling of the transducer to the surface causing removal of the coating. A silicon oxide coating over the aluminium also failed to provide a tough enough as this pulled the aluminium off the surface. The required surface toughness was finally provided by a chromium coating although this did lead to a drop in reflectivity of approximately one third.

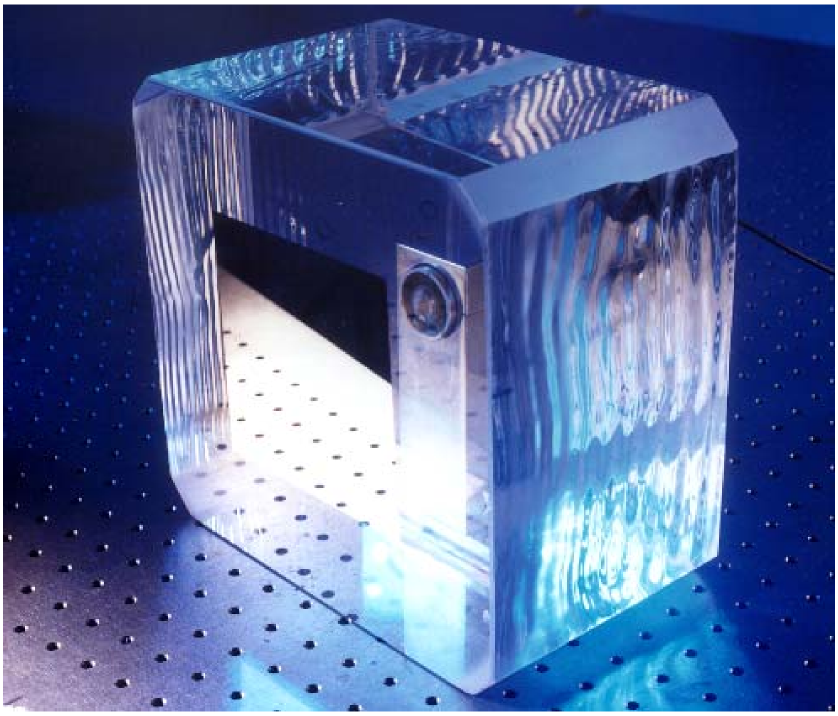

Figure 13. Glass block after polishing and the application of chromium coating.

3.3 Measurement setup

The conical transmitter was coupled to the centre of the chromium coated face of the glass block and a displacement interferometer was positioned on the opposite side of the glass block such that the optical beam reflected from the chromium coating at the contact point of the transmitter after passing through the glass block. This arrangement is depicted in Figure 14 and 15.

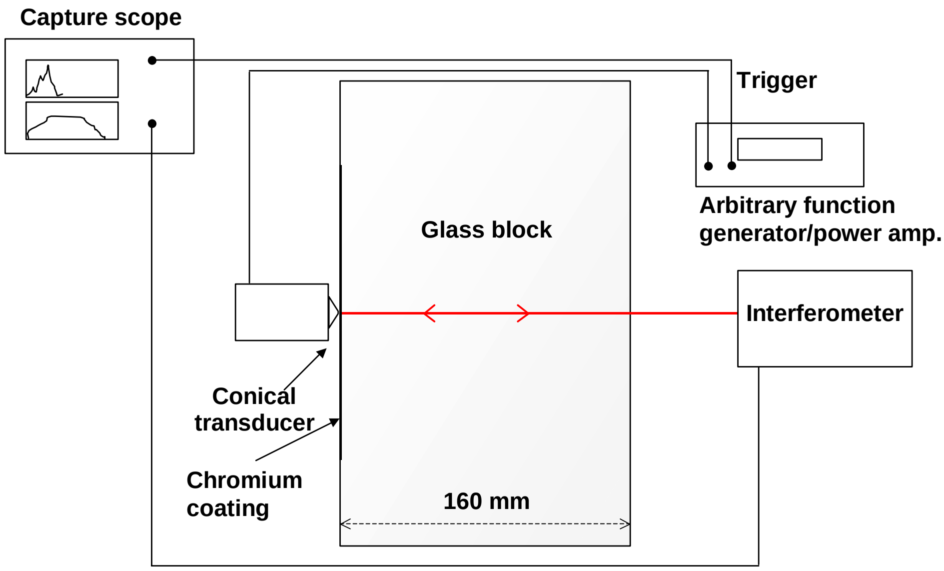

Figure 14. Measurement setup.

The time-of-flight for a compressional wave through the 160 mm thick glass block is approximately 27 µs. In this case, where the transmitter and the laser measurement spot are located in the same position, there will be a measurement window of approximately 54 µs before the arrival of the direct echo from the opposite face. Any reflected surface wave from the corners of the block would be expected around 29 µs after this first echo.

The PCL interferometer used for the measurements is shown in Figure 15 with the conical transmitter coupled to the glass block. This setup allows the interferometer to measure the surface displacement directly at the contact point of the conical transmitter.

A series of measurements were performed to investigate the method of displacement measurement through the glass block using the interferometer, and to further characterise the transmitter. For these measurements, the conical transducer shown in Figure 1 was used as a transmitter and was coupled to the centre of the chromium coated surface with a thin layer of water based coupling gel and held in place with a rigid mount. The transmitter was excited with a steady-state tone-burst, and a short pulse of white-noise source to fully characterise its response to the way in which it might be used in practice. In addition to this, a set of electrical impedance measurements were performed to estimate the resonant behaviour of the transducer.

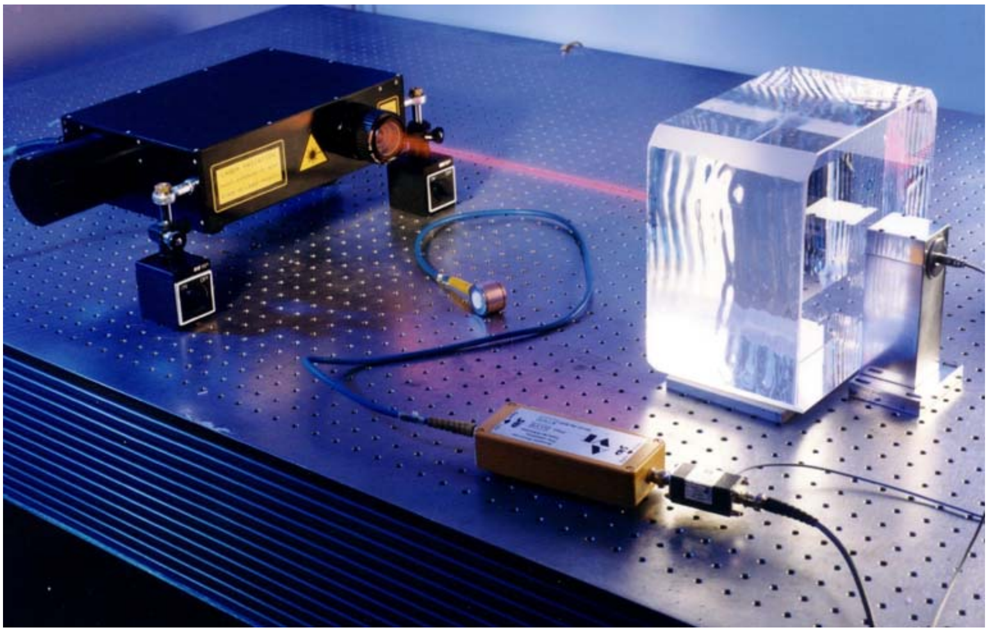

Figure 15. Measurement setup.

4 CHARACTERISATION AND CALIBRATION OF REFERENCE SOURCE

4.1 Impedance analysis

Impedance measurements were performed on the transducer prior to the calibration to identify any resonant components in the transducer response. The measurements were performed using a HP 4924A Precision Impedance analyser where the transducer (including cable) was swept with a continuous wave input of 0.5 Vrms between 1 kHz and 7 MHz at 1 kHz steps. These were performed with the transducer coupled to the centre of the flat face of an aluminium cylinder measuring 260 mm in length with a diameter of 254 mm. Although the impedance of the aluminium would be slightly different to that of the BK7 glass, one would expect the effect of this on the resonant behaviour of the transducer to be minimal. The admittance plot of conductance against susceptance is shown in Figure 16. For a typical resonant transducer one would expect to see a completed admittance loop which would indicate a dominant resonance in the transducers response where the conductance and susceptance values are the same. Figure 16 shows very different behaviour to this, with the susceptance increasing with conductance, where susceptance dominates. This behaviour indicates the transducer is heavily damped, as would be expected with a tungsten epoxy backing, and has no single dominant resonance which would also be expected given the conical design of the element. The transducer does exhibit a number of non-dominant resonances between 250 kHz and 1 MHz.

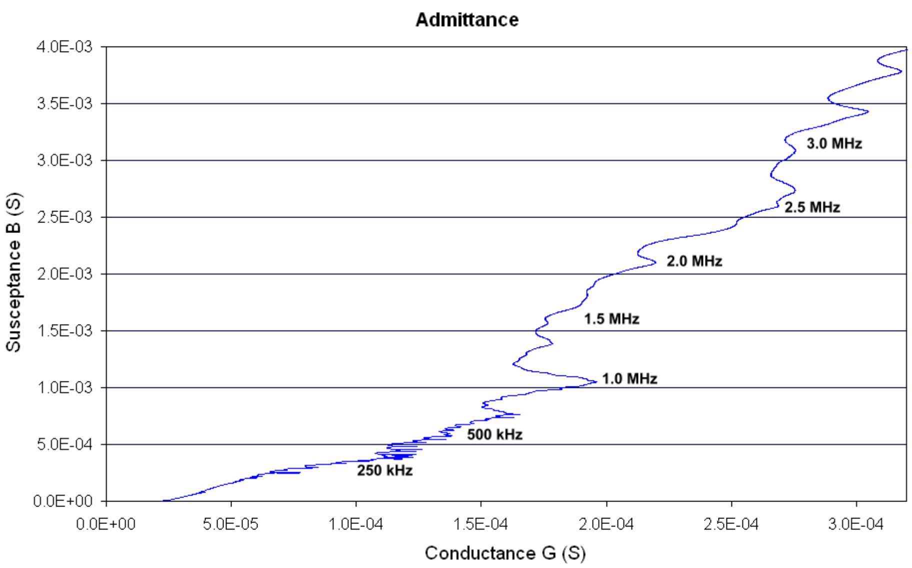

Figure 16. Admittance plot for conical transducer coupled to aluminium cylinder.

4.2 Steady-state excitation

The transmitter was excited with a 100 µs tone-burst using an AG33220A function generator coupled to an ENI 240L 50 dB linear power amplifier to provide a drive level of 50 V_{p-p}. This was performed at a number of frequencies between 50 kHz and 3 MHz at steps of 50 kHz up to 1.2 MHz, at steps of 100 kHz from 1.2 MHz to 2 MHz and then 200 kHz steps up to 3 MHz. The contact displacement for each tone-burst was measured using the PCL self-calibrating interferometer as shown in Figure 15 and captured using a Tekronix TDS 5054 oscilloscope at a sample rate of 125 MHz with 30 time averages. An FFT was then performed on the steady-state region of the time domain waveform. To remove the end effects from the FFT data, the steady-state section of the waveform was windowed prior to FFT analysis using a Tukey window with a 0.1 taper ratio [20]. The full time domain signal from the interferometer and the windowed FFT signal are shown in Figures 17a and 17b respectively for a 100 kHz tone-burst and in Figures 18a and 18b respectively for a 1 MHz tone-burst. The displacement was obtained from the FFT signal to obtain the displacement at the drive frequency component only. This was repeated for each frequency and the results from this analysis are shown in Figure 19. Given that the drive level remained the same throughout the measurements, Figure 19 can be assumed to represent the steady-state transmit response of the transducer on the glass block.

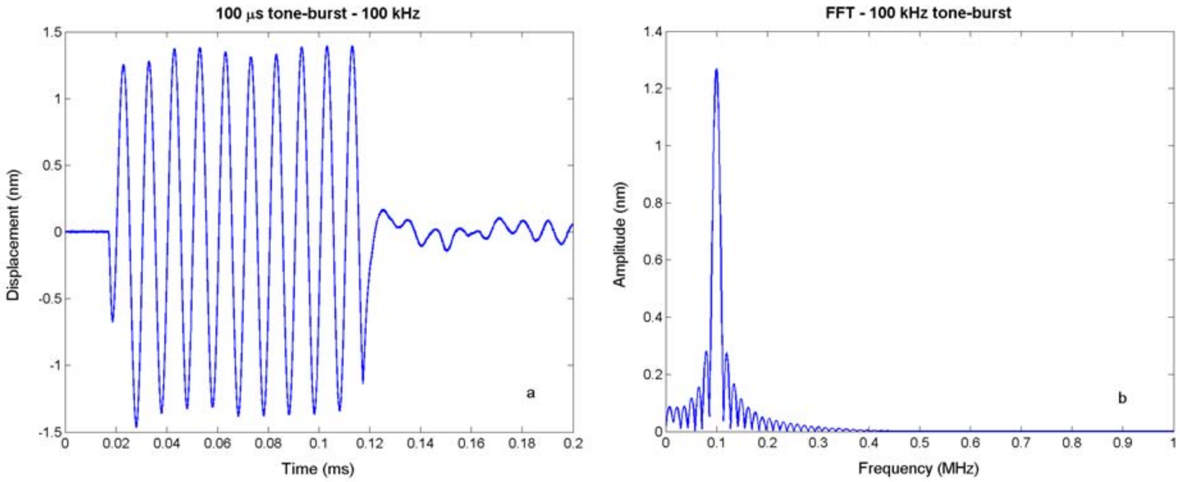

Figure 17. a) 100 kHz tone-burst measured at the conical transmitter. b) FFT of the measured tone-burst.

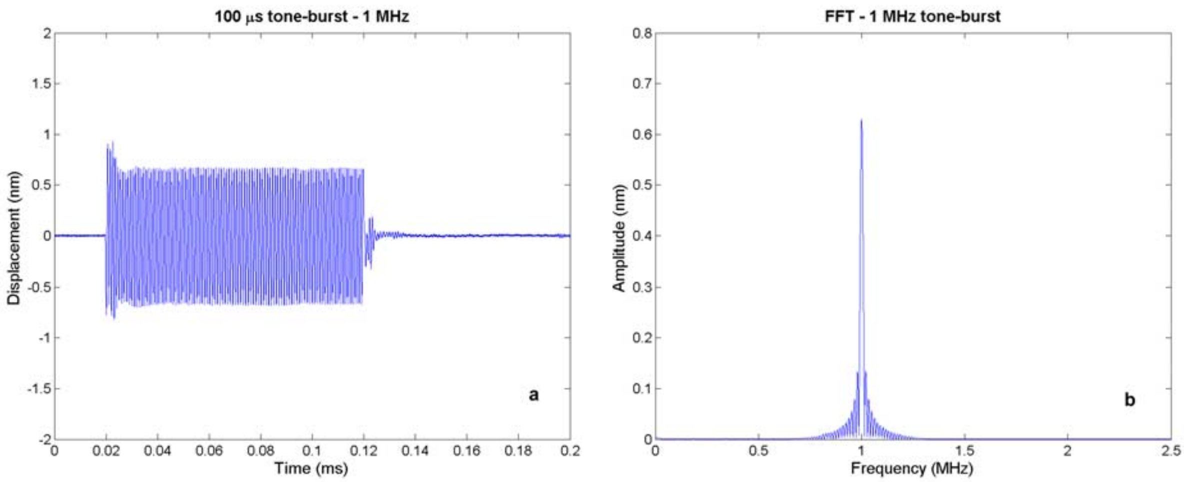

Figure 18. a) 1 MHz tone-burst measured at the conical transmitter. b) FFT of the measured tone-burst.

The steady-state transmit response shown in Figure 19 shows that the transducer does have a number of resonant components, although as suggested in section 2.1 these are not dominant. It was expected that the transducer would have a more sensitive response below 1 MHz due to the radial modes at the top of the cone around 200 kHz and the thickness mode for the 1 mm diameter flat contact area at around 500-600 kHz. The radial mode at the 1 mm contact tip would be expected to produce a small resonance around 1.8 MHz. Other small resonances would be introduced throughout the frequency range due to the conical shape, particularly if there were any ridges present due to the machining of the conical element.

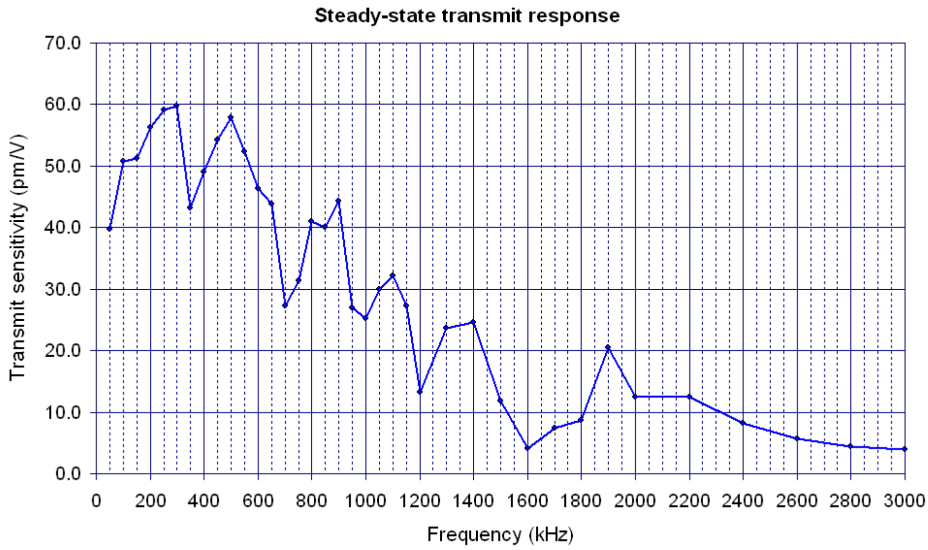

Figure 19. Steady-state transmit sensitivity of conical transducer.

4.3 Pulse excitation

A 250 ns square pulse with a 5 ns rise-time and a potential difference of around 120 V across the transmitter terminals was generated using the AG33220A function generator and the 50 dB ENI 240L power amplifier. The displacement at the centre of the transmitter contact point was again measured using the PCL interferometer and captured using the TDS 5054 oscilloscope using a sample rate of 500 MHz with 100 time averages. The acoustic signal generated at the transmitter contact point was measured using the interferometer, which is shown in Figure 20a, along with the associated windowed FFT signal in Figure 20b. The rise-time of the negative displacement spike generated by the transmitter was measured to be around 0.35 μs which corresponds to a response bandwidth of around 2.8 MHz. The interferometer output plot in Figure 20b also indicates that there is still significant energy generated by the transmitter up to around 2.5 MHz. It should be noted that the reduced output of the transmitter at higher frequencies is partly due to the limited bandwidth generated by the 250 ns input pulse. Figure 20b also shows the FFT of the electrical input signal which highlights the roll-off characteristic of the excitation pulse. It should also be noted that the -3 dB point for the interferometer band-stop frequency is 3 MHz.

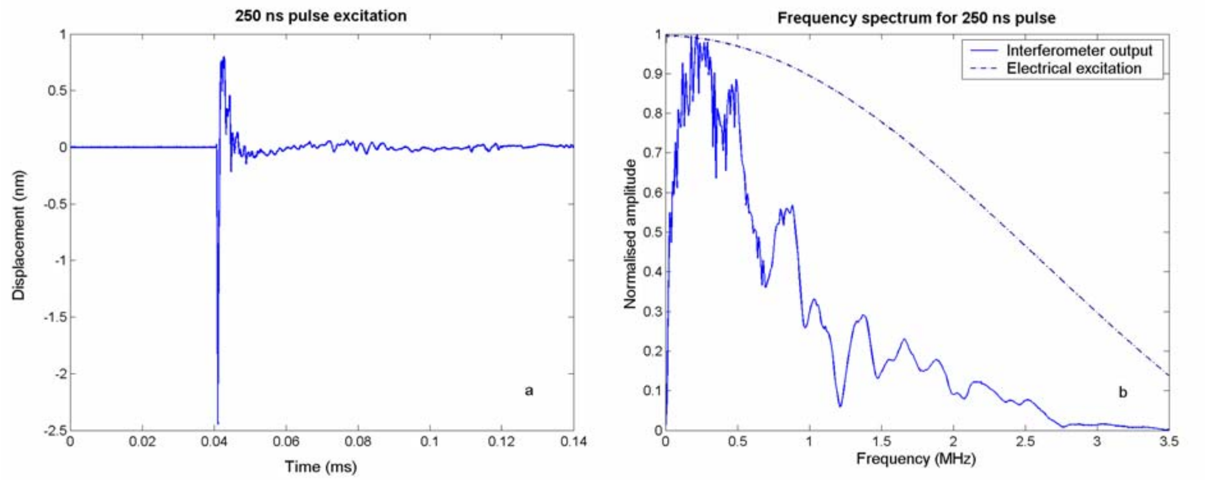

Figure 20. a) 250 ns square pulse excitation measured at the conical transmitter. b) FFT of the measured square pulse excitation.

The pulsed transmit response of the transducer agrees fairly closely with the steady-state transmit response showing resonances around 200 kHz, 500 kHz, 800 kHz and around 1.4 MHz which are caused by a number of radial and thickness modes in the conical element. The heavy damping of the transmitter and the conical design of the active element provide a relatively flat response over a 1 MHz bandwidth.

4.4 Noise excitation

The transmitter was also driven using a broadband 10 Vp-p white-noise source using the AG33220A function generator. The same measurement procedure was used to measure the contact displacement, although no averaging was used in this case and the sample rate was limited to 50 MHz to maximise the measurement period. The noise spectrum obtained from the 1 ms time domain signal following the windowed FFT analysis is shown in Figure 21.

The noise spectrum shows that the broadband response is excellent up to around 1.2 MHz with significant output up to around 2.5 MHz and a response which agrees closely with the steady-state response.

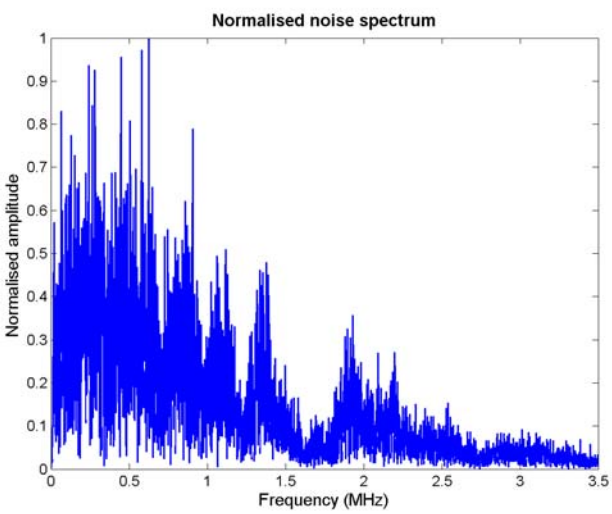

Figure 21. Measured frequency spectrum for white noise excitation of conical transmitter.

5 FUTURE DEVELOPMENT OF REFERENCE SOURCE

5.1 Optimisation of transducer design

The pulse measurement performed in section 4.3 indicated that there were a number of non-dominant resonances present in the transducer response which were thought to be associated with the thickness mode between the back of the element and the 1 mm diameter tip, the radial mode across the top 10 mm diameter of the element and the radial mode across the contact tip 1 mm diameter. The response also seems to be dominated by the radial mode across the larger diameter of the cone, with greater sensitivity between 100 kHz and 500 kHz. Modelling of the transducer using finite element (FE) analysis can provide useful information regarding both the electrical and acoustical characteristics of the transducers. More precisely, the FE analysis can provide information about the vibrational behaviour of the conical element and the effect of the backing mass on the performance of the transducer.

A FE model of the transducer was coded using the PAFEC Vibroacoustics software. The transducer was modelled as an axisymmetric problem with the transducer coupled to a cylindrical glass block. To allow the output of the transducer to be analysed at the contact interface between the transducer and glass block, in the absence of any structural reflections from the boundaries of the glass block, the extremes of the glass block were heavily damped. The mesh shown in Figure 22 shows the damped region in pink.

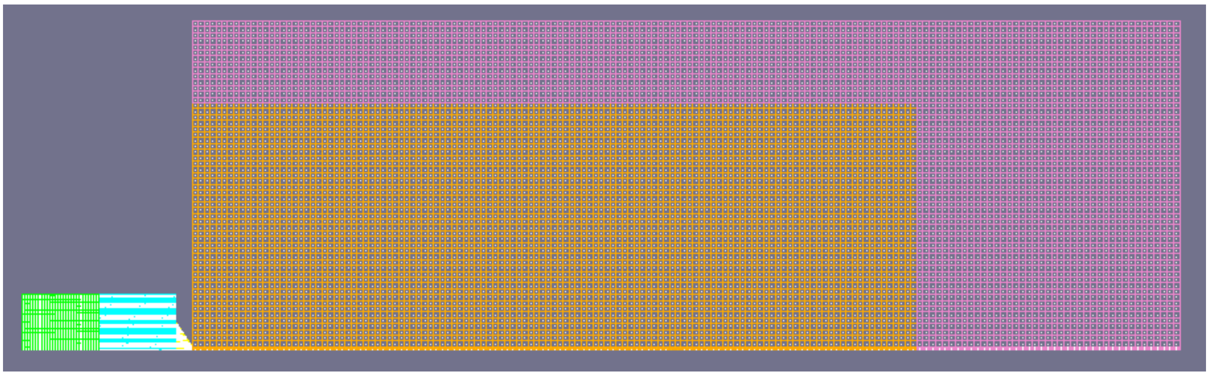

Figure 22. Axisymmetric FE mesh of conical transducer and anechoic glass cylinder.

A transient FE solution for a 500 kHz single cycle sine wave is shown in Figure 23 where the axial displacement is obtained from the centre axis of the transducer/glass block interface. An interferometer measurement using the same excitation and at the same location obtained using the method described in section 3.3 is also shown as a red dotted line in Figure 23.

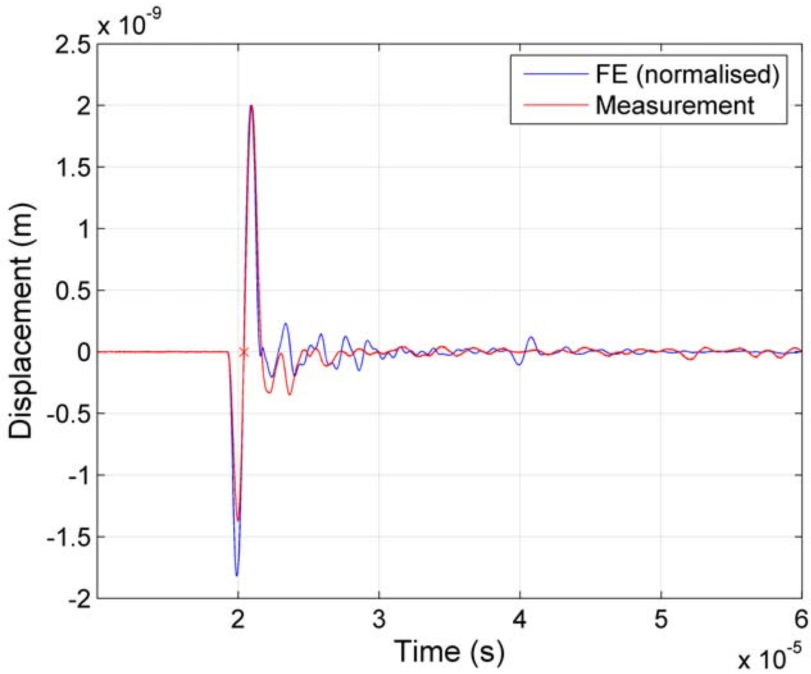

Figure 23. FE output at the conical transducer tip/glass block interface compared with identical interferometer measurement.

The comparison between the two is generally good showing that the model is accurately predicting the behaviour of the transducer. However, the damping factors used in the FE model do need increasing, as the ringing observed in the PZT-5A element (between 2×10^{-5} s and 3×10^{-5} s) was greater than that measured experimentally. The reflection observed at 4x10-5 s in the FE waveform is due to the limited dimensions of the test block coded into the FE model. Although damping was used to remove this, a small surface wave reflection was still present which was not present during the measurement as a larger test block was used.

Although beyond the scope of this report, the FE code of the conical transducer developed will allow different geometries of active element to be considered to provide an optimised design. This will consider a thinner element to increase the central thickness resonance whilst maintaining an optimal aspect ratio for the cone. An improved design might also consider rounded edges at the top of the conical element to reduce the dominance of the low frequency radial modes and also a rounded tip to remove the dominance of the high frequency radial mode and the high frequency thickness mode. This would lead to a smoother response closer to the ideal requirement of approximating the response of step force input.

5.2 Coupling variability

During the reference source calibration, the transducer is coupled to the glass test block using a small amount of water based ultrasonic gel. Given that the surface is optically polished, it is possible to obtain an excellent coupling repeatability, often better than 1%. However, using the reference source to calibrate an actual measurement system would pose significant variability in the coupling. The structures tested using AE techniques are often painted or rusted metal, concrete or painted composite. The use of a different material would introduce an uncertainty due to the load impedance variation, although this would be the same for a given structure and could be corrected for analytical techniques. However, the uncertainty due to coupling the reference source to a given structure could be large, possibly up to 30% for poor condition surfaces.

Previous work in the literature [7,18,21] has suggested that a double element transducer design can provide some indication of the transducer coupling efficiency with the contact surface. The double element design used a standard conical transducer with a second piezoelectric element bonded to the backing mass of the transducer. The active conical element acted as the transmitter and the second piezoelectric element acted in a passive nature, where its output was in some way a function of the coupling efficiency of the conical element with the test structure.

This milestone also considered such a design with Brunel University where the transducer was a simple modification of a brass-backed conical transducer. The brass-backed conical transducer was identical to the tungsten epoxy-backed conical transducer except for the dimensions and material properties of the mass backing. The transducer was modified by the bonding of a second transducer to the top of the brass backing. The construction of the double element transducer is shown in Figure 24.

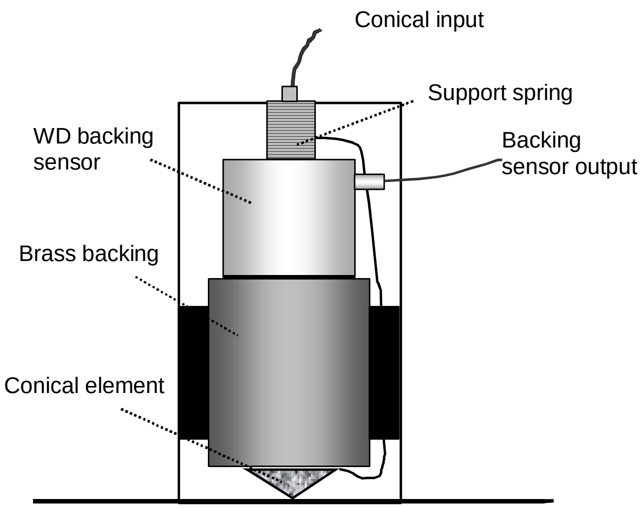

Figure 24. Construction of double element transducer.

The second element used in the double element transducer was a PAC WD transducer permanently bonded to the brass backing using Loctite superglue. The brass, although having a better impedance match to the PZT material, offered poorer damping due to its lower attenuation than tungsten epoxy. The brass-backed transducer was used for convenience and also because of the high attenuation of the tungsten epoxy allowing very little transmission through the backing.

Although there clearly exists a relationship between the coupling efficiency of the transducer with the specimen [9] and the output of the backing sensor, the relationship is not completely understood. It has been proposed in the literature [18] that stiffening of the transducer by mechanical loading due to better coupling leads to an overall increase in the resonant frequency of the the transducer. The result is that below the resonant frequency of the transducer, an improved coupling efficiency leads to a reduction in amplitude at the backing sensor. Above the resonant frequency of the transducer, the result is the inverse of this.

To try and better understand the relationship between the coupling efficiency or contact stiffness and the output from the backing transducer it was decided to produce a simple mass spring model of the double element transducer. Methods for modelling coupling layers by the use of a spring to represent the contact stiffness have been investigated in the literature [22,23] where the aim was to determine the contact stiffness between two contacting surfaces, for ultrasonic inspection by measurement of the reflected component. It was considered that a similar approach could be used for modelling this type of double element transducer for very good coupling conditions. Therefore, a simple two-degree-of-freedom mass spring model has been produced for the double element transducer shown in Figure 24, where the contact stiffness is represented by the spring of stiffness k_c. A representation of the model is shown in Figure 25, where k_1 represents the supporting force spring at the back of the transducer where m_1 and k_2 represent the backing sensor mass and PZT element. m_2 and k_3 represents the brass backing and the conical PZT element in contact. The transducer/surface coupling or the contact stiffness is represented by the spring k_c; x_1 and x_2 represent the displacements of m_1 and m_2 respectively. A force $F(t)$ is applied to the conical transducer that represents excitation of the transducer by a voltage.

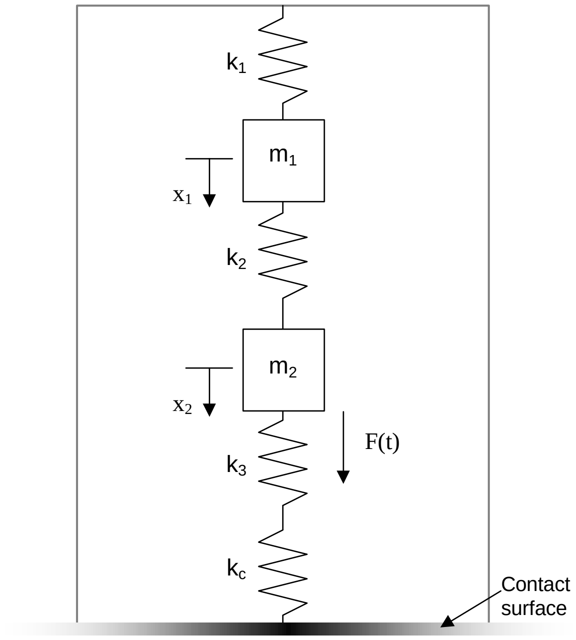

Figure 25. Mass-spring model representation of double element transducer.

The mass-spring system depicted in Figure 25 can be described by the following ordinary differential equations:

$$m_1.\frac{d^2x_1}{dt^2} + (k_1 + k_2).x_1 - k_2.x_2 = 0 \quad (1a)$$

$$m_2.\frac{d^2x_2}{dt^2} + k_2.x_1 + (k_2 + k_{3c}).x_2 = F(t), \quad (1b)$$

where $F(t)$ is an impulse force described by a Dirac function, k_{3c} is a resultant spring constant from a series combination of k_3 and k_c given by:

$$k_{3c} = \frac{k_3 + k_c}{k_3.k_c}. \quad (2)$$

Solving the differential equations given in equation 1a and 1b for $x_1(t)$ and $x_2(t)$ with zero initial conditions for both displacements and velocities gives,

$$x_1(t) = \frac{\omega_{bsq}}{m_2}.\left[\frac{-1}{(A-B).(A+B).A}.\sin(A.t) + \frac{1}{(A-B).(A+B).B}\sin(B.t)\right] \tag{3a}$$

$$x_2(t) = \frac{1}{m_2}.\left[\begin{array}{l} \frac{1}{(A-B).(A+B)}.A.\sin(At) - \frac{1}{(A-B).(A+B).A}.\sin(At).\omega_{asq} \\ -\frac{1}{(A-B).(A+B)}.B.\sin(Bt) + \frac{1}{(A-B).(A+B).B}.\sin(Bt).\omega_{asq} \end{array}\right] \tag{3b}$$

The coefficients A and B are given by,

$$A = \sqrt{\frac{1}{2}.\omega_{asq} + \frac{1}{2}.\omega_{csq} - \frac{1}{2}.\left(\omega_{asq}^{\ 2} - 2.\omega_{csq}.\omega_{asq} + \omega_{csq}^{\ 2} + 4.\omega_{bsq}^{\ 2}\right)^{\frac{1}{2}}} \tag{4a}$$

$$B = \sqrt{\frac{1}{2}.\omega_{asq} + \frac{1}{2}.\omega_{csq} + \frac{1}{2}.\left(\omega_{asq}^{\ 2} - 2.\omega_{csq}.\omega_{asq} + \omega_{csq}^{\ 2} + 4.\omega_{bsq}^{\ 2}\right)^{\frac{1}{2}}} \tag{4b}$$

where $\omega_{asq} = (1+\kappa_{21}).\omega_{11}^{\ 2}$, $\omega_{bsq} = \frac{\kappa_{21}}{\mu_{21}}.\omega_{11}^{\ 2}$, $\omega_{csq} = \left(\frac{\kappa_{21}+\kappa_{3c1}}{\mu_{21}}\right).\omega_{11}^{\ 2}$ and $\omega_{11}^{\ 2} = \frac{k_1}{m_1}$. κ and μ are the respective spring constant and mass ratios for the corresponding spring and mass numbers.

The relative displacements across k_2 and k_3, which represent the displacements across the backing and conical crystal respectively can be given in terms of x_1 and x_2 by,

$$z_2 = (x_1 - x_2) \tag{5}$$

$$z_3 = x_2.\frac{k_c}{(k_3 + k_c)} \tag{6}$$

Since the conical PZT backing mass is brass and the backing sensor has minimal damping, the damping in the transducer should actually be relatively low. To keep the solution as simple as possible it was therefore chosen not to add damping components to the model. A spring constant of 5000 N/m was used for k_1, based on a measurement of the force required to compress the spring by the 2 mm compression it undergoes when the transducer is secured to a test surface. The spring constants k_2 and k_3 were chosen based on estimates for PZT 5A of 1.1×10^8 N/m in the literature [24,25]. Mass m_1 and m_2 were both measured, respectively giving 0.04 kg for the mass of the backing sensor and 0.045 kg for the mass of the brass backing. This provides a resonant frequency of the transducer of around 13 kHz, which is somewhat lower than that for the actual 3 mm thickness resonant tuned device. Although not providing a quantitative description of the transducer or its frequency response, the model should still allow for a relative evaluation of the behaviour of the device for varying values of contact stiffness.

For an initial impulse amplitude z_2 and z_3 were obtained for a series of contact stiffness values, k_c. The active element of the double element transducer contacts the test surface together with a relatively small force and so it is thought that the contact stiffness would be somewhat less than that predicted in the literature for surfaces contacting under pressure [22,23]. Amplitudes for the backing element, z_2, and the conical element, z_3, as a function of contact stiffness values from zero up to 1×10^6 N/m are shown in Figures 26 and 27 respectively.

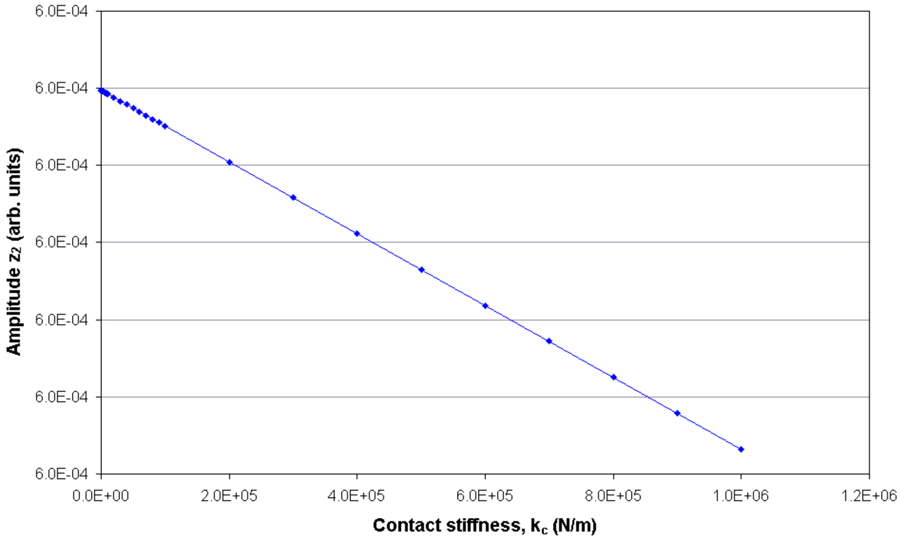

Figure 26. Amplitude at the backing element as a function of contact stiffness.

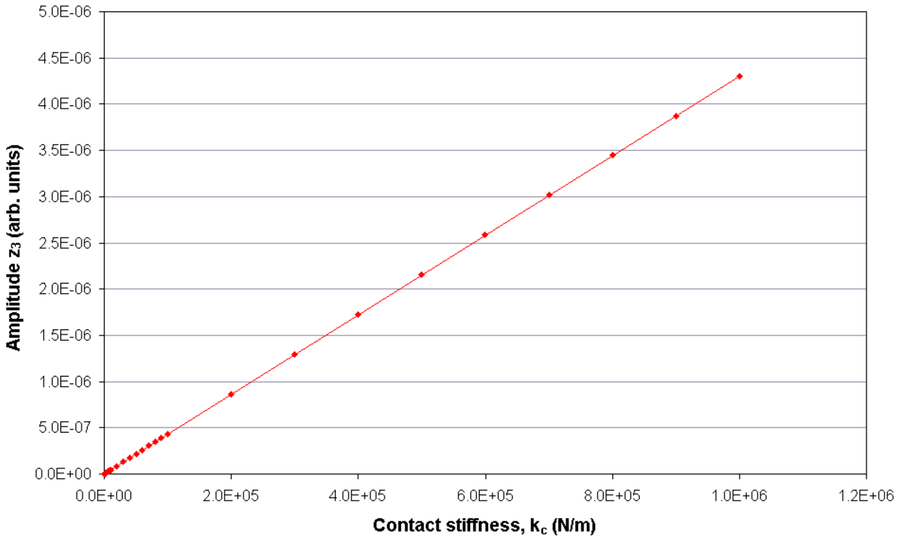

Figure 27. Amplitude at the conical element as a function of contact stiffness.

Figures 26 and 27 show that for an impulse input, the amplitude at the backing element, z_2, reduces linearly with increasing contact stiffness, whilst the amplitude at the conical element, z_3, increases linearly with increasing contact stiffness. This is highlighted in Figure 28, where the amplitude at the conical element, z_3, is plotted as a function of the amplitude at the backing element, z_2, values of contact stiffness ranging from zero to 1×10^6 N/m.

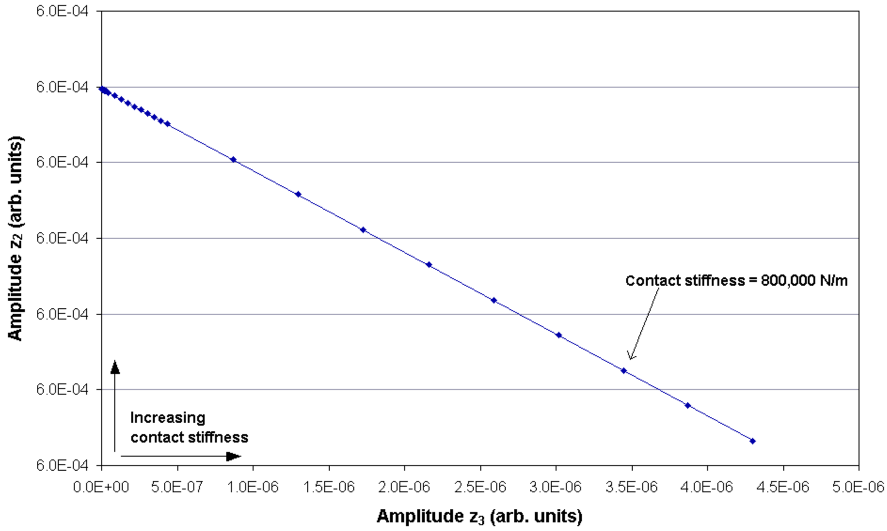

Figure 28. Relationship between z_2 and z_3 for contact stiffness values between zero and 1×10^6 N/m.

The efficiency of the coupling or the contact stiffness acts to change the resonant frequency of the transducer [18] where the overall effect is to increase the resonant frequency of the transducer as the coupling efficiency or contact stiffness is increased. The model showed this trend to be true and also showed a linear increase for the stiffness contact range used, as is shown in Figure 29. The contact stiffness range shown in Figure 29 is thought to cover a much greater range than the variation encountered through inconsistent coupling of the transducer. In reality therefore, the resonant frequency change would be expected to be small, which in practice may be difficult to quantify.

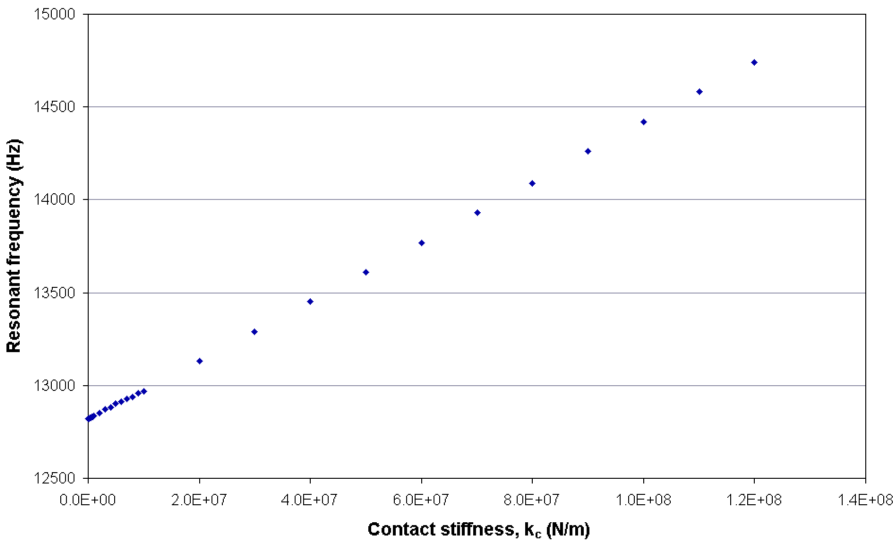

Figure 29. Transducer resonant frequency as a function of contact stiffness.

Note that the maximum contact stiffness used in Figure 29 is around 2 orders of magnitude greater than the maximum used in Figure 26 to 28, exceeding the spring stiffness used to represent the PZT 5A elements. Increasing the contact stiffness has a different effect on the amplitudes of the conical element, z_3, which begins to show a levelling off with increasing contact stiffness. As the contact stiffness approaches that of the PZT spring constant, the linear relationship breaks down. This is shown in Figure 30 up to a contact stiffness of 1.2 x 10^8 N/m however, the amplitude at the backing element, z_2, remains linear.

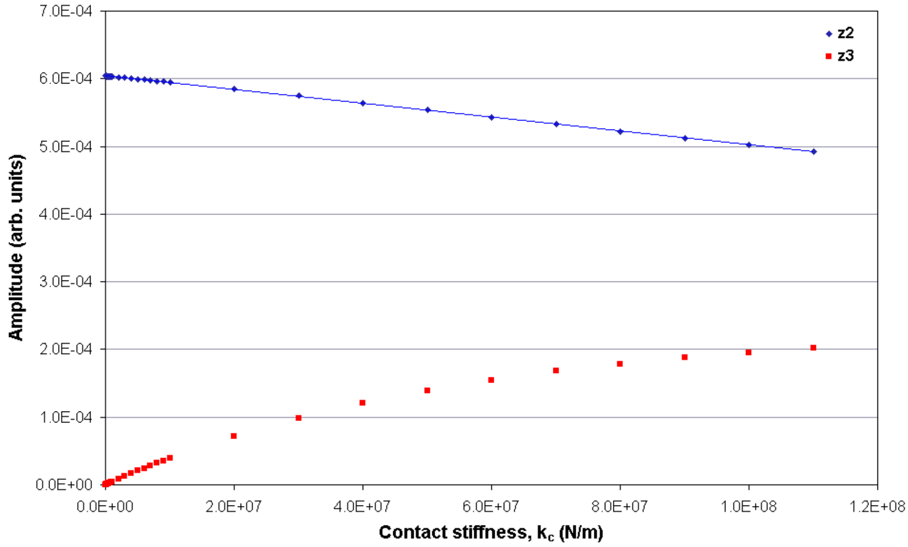

Figure 30. Amplitude z_2 and z_3 as a function of contact stiffness up to 1.2 x 10^8 N/m.

Increasing the contact stiffness further showed a turn around in the relationship between the conical amplitude, z_3, and the contact stiffness. It also showed that the linear relationship between the backing amplitude, z_2, and the contact stiffness ceases. Figure 31 shows these changes and the fact that once the contact stiffness becomes very stiff, the amplitudes z_2 and z_3 tend to the same value.

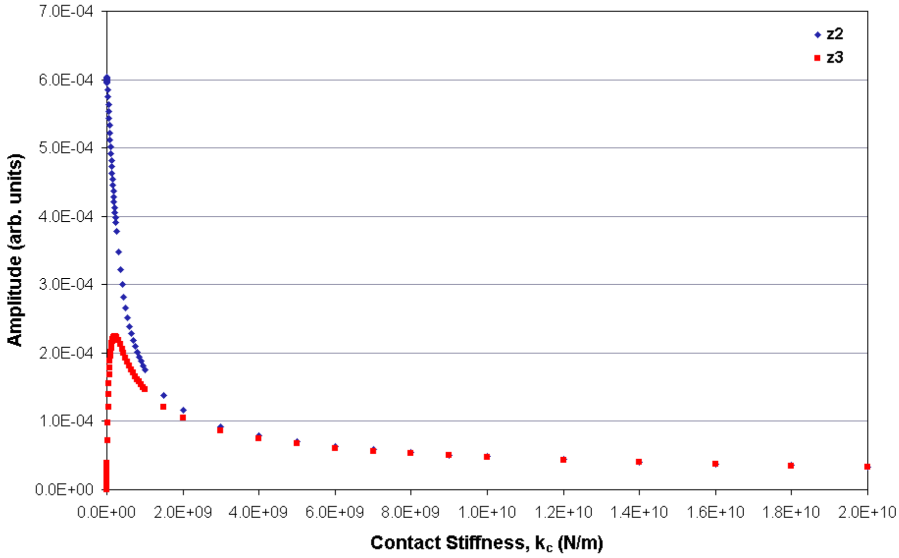

Figure 31. Amplitude z_2 and z_3 plotted for a large range of contact stiffness values.

It is thought that the contact stiffness as a result of coupling the transducer to the surface will in this case be small compared with the values used in Figure 31. For less stiff contacts and for a relatively small variation in contact stiffness as a result of inconsistent couplings, it is probable that the variation of z_2 and z_3 with contact stiffness will remain linear.

Measurements performed as part of this milestone and a previous Strategic Research Project have shown the relationship between the output of the backing sensor and the output measured by a sensor coupled directly to the test block to which the double element transducer was coupled [9]. The measurements showed that there clearly exists an inverse linear relationship between the backing sensor output and the coupling efficiency of the transducer (determined using a sensor coupled to the test block) which agrees with that predicted by the relative model in Figure 26. Figure 32 shows the output of the backing sensor for the case when the double element transducer is coupled to an aluminium slab (Figure 32b) and when it is unloaded in air (Figure 32a).

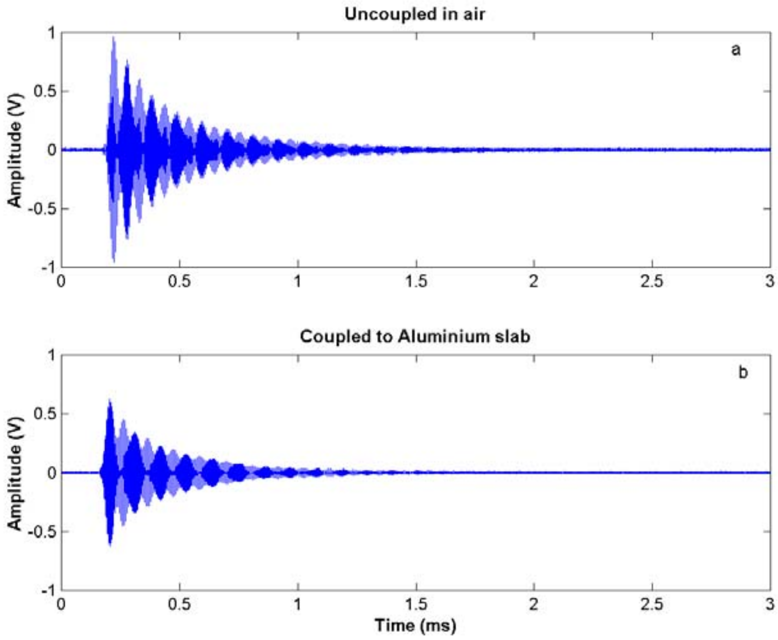

Figure 32. a) Uncoupled output from backing element. b) Coupled output from backing element.

The output waveform from the backing element of the coupled double element transducer shows a significant drop in amplitude compared with the uncoupled case as predicted by the results from the model shown in Figure 26. The change in resonance predicted by the model was difficult to identify in this case and difficult to relate to amplitude change, given the number of resonant components present and the internal ringing of the transducer. It does however show that amplitude or decay time could be used to predict the difference between good coupling and a poor coupling.

5.3 Robustness

For the transducer to be useful as a reference source, the transducer has to exhibit the robustness necessary for industrial use. The present design does not provide this as the PZT element is exposed and the electrical contact is provided by a thin brass shim, which also provides the only protection for the delicate tip of the active element. Future work needs to consider a contained design which does not compromise the point contact operation of the transducer and enables the transducer to not only survive the rigors of industrial use but also remain unchanged between calibration periods.

6 CONCLUSIONS

6.1 Summary

A design of conical transducer has been demonstrated as a potential reference source which could be used for the calibration of acoustic emission measurement systems. This device should provide a metrologically sounder test of the AE equipment, than the conventionally applied pencil lead break. The conical transducer can provide a versatile input to a structure, either providing a pulse input with similar rise-time characteristics to the pencil lead break or a range of tone-burst type inputs over a range of frequencies. The transducer provides substantial transmit sensitivity between 50 kHz and 1.5 MHz and also offers complete control over the input displacement.

This report has also demonstrated a methodology for calibration of the conical transducer using a glass test block and displacement interferometer enabling the transducer to provide a known input displacement to a structure for a given excitation voltage. At this stage the reference source requires further work to optimise its design and robustness and to develop a method of monitoring the coupling when the reference source is used for calibration of AE measurement systems.

6.2 Future work

For the reference source to be a useable and useful calibration tool for industrial users a number of elements of the transducers design and construction need to be further developed. The following provides a list of design and construction changes which are planned as part of the 2004-2007 NMS Acoustical Metrology Programme which should provide greater robustness, improve the broadband frequency output and allow the reference source to provide a known input under varying surface and material conditions:

- Active element and backing mass design optimisations using Finite Element modelling

- Re-design of transducer coupling face to improve coupling consistency

- Re-design of transducer packaging for greater robustness

- Integration of a monitoring capability to determine quality of coupling

7 ACKNOWLEDGEMENTS

We gratefully acknowledge the financial support of the UK Department of Trade & Industry (National Measurement System Directorate).

8 REFERENCES

[1] N. N. Hsu, US Patent 4, 018, 084 (1977).

[2] J. T. Barnett, R. B. Clough and B. Kedem, *Power considerations in acoustic emission*, J. Acoust. Soc. Am., Vol. 98, No. 4, pp 2070-2081, 1995.

[3] R. B. Clough, *The energetics of acoustic emission source characterisation*, Mat. Eval.,Vol. 45, No. 5, pp 556-563, 1987.

[4] Y. Berlinsky, M. Rosen, J. Simmons and H. N. G. Wadley, *A calibration approach to acoustic emission energy measurement*, J. Non-destructive Eval., Vol. 10, No. 1, pp 1-5, 1991.

[5] R. B. Clough, *A scalar approach to acoustic emission*, Winter Annual Meeting of the American Society of Mechanical Engineers - Noise Control and Acoustics Division, Vol. 14, pp 101-110, 1992.

[6] C. B. Scruby and L. E. Drain, *Laser ultrasonics*. Bristol: Adam Hilger, 1990.

[7] T. Yan, P. Theobald and B. E. Jones, *A self-calibrating piezoelectric transducer with integral sensor for in situ energy calibration of acoustic emission*, NDT&E International, Vol. 35, pp 459-464, 2002.

[8] P. D. Theobald, *Towards traceable calibration of acoustic emission measurement systems: Development of a reference source a the UK's National Physical Laboratory*, Proceedings of the 26th European conference on acoustic emission testing, Band 2, pp 833-842, 2004.

[9] T. Yan, P. Theobald and B. E. Jones, *A conical piezoelectric transducers with integral sensor as self-calibrating acoustic emission energy source*, Ultrasonics, Vol. 42, pp 431-438, 2004.

[10] T. M. Proctor, *An improved piezoelectric acoustic emission transducer*, J. Acoust. Soc. Am., Vol. 71, No. 5, pp 1163-1168, 1982.

[11] T. M. Proctor, *Some details on the NBS conical transducer*. J. Acoust. Emiss. Vol. 1, pp 1173-1178, 1982.

[12] T. M. Proctor, *More-recent improvements on the NBS conical transducer*. J. Acoust. Emiss. Vol. 5, pp 134-142 1986.

[13] M. Greenspan, *The NBS conical transducer: Analysis*, J. Acoust. Soc. Am., Vol. 81, No. 1, pp 173-183, 1987.

[14] C. B. Scruby, *Acoustic emission measurement using point-contact transducers*, AERE Harwell internal report AERE-R 11328 (1984).

[15] D. A. Hutchins, L. F. Bresse and S. B. Palmer, *Measurements with a thick piezoelectric transducer*, J. Acout. Soc. Am., Vol. 85, No. 6, pp 2417-2422, 1989.

[16] Y-C. Lee and S. H. Kuo, *A new point-source/point receiver acoustic transducer for surface wave measurement*, Sensors and Actuators A, pp 129-135, 2001.

[17] Y-C. Lee and S. H. Kuo, *Miniature conical transducer realized by excimer laser micro-machining technique*, Sensors and Actuators A, pp 57-62, 2001.

[18] M, Evans, *The use of diffuse field measurements for acoustic emission*, Ph D thesis, Imperial College of Science and Technology, London, 1997.

[19] T. J. Esward, P. D. Theobald, S. P. Dowson and R. C. Preston, *An investigation into the establishment and assessment of a test facility for the calibration of acoustic emission sensors*, NPL Report CMAM 82, 2002.

[20] F. J. Harris, *On the Use of Windows for Harmonic Analysis with the Discrete Fourier Transform*, Proceedings of the IEEE. Vol. 66, pp. 66-67, 1978.

[21] M. J. Evans, J. R. Webster and P, Cawley, *Design of a self-calibrating simulated acoustic emission source*, Ultrasonics, Vol. 37, pp 589-594, 2000.

[22] B. W. Drinkwater, R. S. Dwyer-Joyce and P. Cawley, *A study of the interaction between ultrasound and a partially contacting solid-solid interface*, Proc. R. Soc. Lond., Part A, Vol. 452, pp 2613-2628, 1996.

[23] K. Hodgson, R. S. Dwyer-Joyce and B. W. Drinkwater, *Ultrasound as an experimental tool for investigating engineering contacts*, *Tribologia - Finnish Journal of Tribology*, Vol. 19, No. 4, pp 9-17, 2000.

[24] M. A. Hampstead and C. M. Fortunko, *Development of practical wideband high fidelity acoustic emission sensors,* Nondestructive evaluation of ageing bridges and highways: 6-7 June 1995, Oakland, California SPIE proceedings vol. 2456, 1995.

[25] S. D. Glaser, G. G. Weiss and L. R. Johnson, *Body waves recorded inside an elastic half-space by an embedded, wideband velocity sensor*, J. Acoust. Soc. Am., Vol. 104, No. 3, pp 1404-1412, 1998.